Journal of Science and Technology – Smart Systems and Devices
Volume x, Issue x, Month Year, ppp–ppp

Thermo-Physical Interpretation and Predictive Optimization of Material Removal Rate in Die-Sinking Electrical Discharge Machining of Hardened SKD61 Steel Using an Using a Response Surface Methodology–Particle Swarm Optimization Framework

That Nguyen Huu, Chien Vu Ngoc*
Faculty of Mechanical Engineering, Nha Trang University, Khanh Hoa, Vietnam
**Corresponding author email: chienvn@ntu.edu.vn*

Abstract

Electrical discharge machining (EDM) is indispensable for producing complex cavities in hardened tool steels, yet reliable productivity prediction remains challenging owing to the strongly nonlinear dependence of material removal rate (MRR) on discharge settings. This study investigates MRR in die-sinking EDM of hardened SKD61 steel (50 HRC) using a cylindrical copper electrode. An L_{27} (3^3) design comprising all 27 unique combinations was used to characterize the effects of current-rate index I (5-11), gap voltage V (50-70 V), and time on index T_{on} (3-7) on MRR; the controller indices are reported without conversion to amperes or pulse duration. A full second-order response surface model (RSM) fitted by least-squares regression achieved $R^2 = 0.995$, Adj-$R^2 = 0.993$, and Pred-$R^2 = 0.988$. Current-rate index was the dominant factor, and the fitted quadratic and interaction trends were interpreted as being consistent with literature-established thermal-erosion mechanisms rather than as direct measurements of plasma or debris behavior. Particle swarm optimization (PSO; 40 particles, 50 iterations) identified the boundary setting I = 11, V = 50 V, and T_{on} = 3, with a model prediction of 38.33 mm³/min. Three independent confirmation trials produced 37.85, 37.52, and 37.64 mm³/min (mean 37.67 ± 0.17 mm³/min), corresponding to a 1.75% model overprediction; no improvement over the best L_{27} result is claimed. The contribution is a setting-faithful, experimentally confirmed MRR optimization for hardened SKD61 with a literature-grounded interpretation of the full quadratic response.

Keywords: Electrical discharge machining, hardened SKD61 steel, material removal rate, particle swarm optimization, response surface methodology, thermal erosion mechanism.

In press

1. Introduction

Electrical discharge machining (EDM) is a non-conventional material-removal process that erodes electrically conductive workpiece material through a controlled sequence of spark discharges in a dielectric medium [1]. Unlike conventional cutting, EDM exerts no macroscopic cutting force on the workpiece, making it the preferred process for shaping intricate cavities in hard, brittle, or thermally sensitive materials [2]. Its industrial importance is reflected by its pervasive use in die and mould manufacturing, aerospace component finishing, and the production of medical devices and micro-electromechanical systems [3, 4].

Material removal in EDM proceeds through a sequence of transient plasma events. When the voltage across the inter-electrode gap exceeds the dielectric breakdown strength, a plasma channel forms, reaching temperatures of 8,000-12,000 °C and delivering an intense heat flux to the workpiece surface [5]. DiBitonto *et al*. [5] established a cathode erosion model in which crater volume is proportional to the incident heat flux integrated over the pulse duration, while Eubank *et al*. [6] demonstrated that the plasma channel radius expands throughout the pulse, progressively diluting the surface heat flux. The interplay between these two phenomena-energy input and flux dilution-is the physical basis for the nonlinear dependence of MRR on discharge current and pulse-on time observed across EDM studies.

Hot-work tool steel SKD61 (equivalent to AISI H13) is relevant to die and mould manufacturing, where complex cavities in hardened materials are commonly produced by EDM [1]. Previous work on AISI H13 examined productivity, quality, and cutting energy in hard milling under nanofluid minimum quantity lubrication [7]. The present study focuses on MRR in die-sinking EDM of hardened SKD61.

Systematic characterization of EDM process behavior has been pursued extensively through design of experiments (DOE) and statistical modeling. Full factorial and central composite designs have been applied to characterize parameter effects in micro-EDM drilling and die-sinking EDM [8, 9]. EDM parameter effects have also been studied for WC–Co [10] and toolsteel surface roughness [11]. Response surface methodology (RSM) fits continuous polynomial models

p-ISSN 3093-3285
e-ISSN 3093-3315
https://doi.org/10.51316/jst.xxx.ssad.xxxx.xx.x.x
Received: Jul 18, 2026; Revised: Aug 27, 2026;
Accepted: Sep 17, 2026; Online: Nov 11, 2026

that capture linear, quadratic, and two-factor interaction effects, enabling analytical optimization and graphical interpretation of multi-factor behavior [12, 13]. RSM applications include Al-matrix composites [13], mixed-oxide ceramics [14], AISI D2 tool steel [15], and dry EDM [16]. These studies establish RSM as a modeling framework for EDM process characterization.

Beyond statistical characterization, metaheuristic optimization algorithms have increasingly been coupled with RSM surrogate models to improve process efficiency. Particle swarm optimization (PSO), introduced by Kennedy and Eberhart [17], mimics the collective search behavior of biological swarms and is well suited to continuous, non-convex engineering optimization problems. Dang [18] demonstrated its effectiveness for constrained multi-objective EDM optimization using a kriging surrogate. Subsequent work has employed grey relational analysis combined with RSM [19], machine-learning regressors for wire-EDM [20], and multi-criteria decision frameworks [21, 22]. Because these workflows are already established, the methodological combination itself is not presented here as fundamentally new. A recurring opportunity is to connect fitted statistical trends to the underlying erosion physics while keeping the resulting claims proportional to the measurements available.

The present study therefore focuses on a setting-faithful analysis of MRR in die-sinking EDM of hardened SKD61 (50 HRC). An L_{27} (3^3) design is used to cover all 27 combinations of three controller settings, a full second-order RSM is fitted, and PSO is applied within the tested domain. The specific contribution is the combination of transparent controller-index reporting, independent experimental confirmation of the model-selected setting, and a literature-grounded thermo-physical interpretation of the fitted quadratic and interaction trends. The objectives are: (i) to develop and cross-validate a predictive model for MRR, and (ii) to assess whether the statistical trends are consistent with established plasma-channel concepts [5, 6]. The optimization is intentionally limited to productivity through MRR; surface roughness, electrode wear, and surface integrity are outside the response set of this study.

2. Materials and Methods

2.1. Workpiece Material and Electrode Configuration

Hardened SKD61 tool steel (AISI H13 equivalent, 50 HRC as confirmed by Rockwell hardness testing at five locations across each specimen face) was used as the workpiece material. The typical chemical composition is listed in Table 1. Rectangular specimens of 50 mm × 50 mm × 20 mm were sectioned from a single commercially produced bar to eliminate inter-block material variability. Hardening was performed by vacuum quenching at 1,020 °C, followed by double tempering.

A cylindrical copper (Cu) electrode of 12 mm diameter was mounted on the *Z*-axis of a TOPEDM CNC430/X600 die-sinking EDM machine (rated maximum current 75 A). The machine reports current rate as a controller index; the selected levels therefore must not be interpreted as direct ampere values. Copper was selected for its high electrical and thermal conductivity [23, 24]. Commercial EDM oil served as the dielectric fluid. The workpiece was connected positive and the electrode negative ($J = 1$), with the copper-to-steel pairing K1. Controller settings L1, G5, H4, and servo sensitivity 3 were held constant, and lateral flushing pressure was maintained at 0.1 MPa for every run.

Table 1. Typical chemical composition of SKD61 steel (mass%) [25]

Element	C	Si	Mn	Cr	Mo	V
% weight	0.38	1.00	0.45	5.00	1.20	1.00

2.2. Experimental Design

An L_{27} (3^3) design comprising all 27 unique combinations of three factors at three levels was employed: current-rate index I (5, 8, and 11), gap voltage V (50, 60, and 70 V), and time on index T_{on} (3, 5, and 7). Each of the 27 design points was machined once, with no replicate runs in the model-fitting data set. The levels were established from machine recommendations and preliminary stability trials. Each experiment produced a cylindrical cavity of 12 mm nominal diameter and 2 mm depth, and the machining time was recorded electronically. Run order was randomized to mitigate systematic temporal drift.

2.3. Material Removal Rate Measurement and Response Surface Methodology Formulation

MRR was calculated from the nominal cylindrical cavity volume divided by the measured machining time t_m (min):

$$MRR = \frac{\pi D^2 h}{4t} \quad (1)$$

where D = 12 mm, h = 2 mm

This formulation is consistent with the approach adopted by Singh *et al*. [24] and yields MRR in mm³/min. A full second-order RSM model was fitted by ordinary least-squares regression to the coded factor values $x_i \in \{-1, 0, +1\}$:

$$MRR = \beta_0 + \Sigma\beta_i x_i + \Sigma\beta_{ii} x_i^2 + \Sigma\Sigma\beta_{ij} x_i x_j \quad (2)$$

Model adequacy was assessed using R^2, adjusted R^2 (Adj-R^2), predicted R^2 (Pred-R^2) calculated from the PRESS statistic, and residual/influence

In Press

diagnostics [12, 15]. Because each of the 27 unique design points was run once, pure experimental error could not be estimated separately; consequently, a conventional pure-error lack-of-fit test was not used.

2.4. Particle Swarm Optimization

PSO was implemented in MATLAB (R2023b). The swarm comprised 40 particles with a maximum of 50 iterations. Cognitive and social acceleration coefficients were $c_1 = c_2 = 2.0$ [17], and inertia weight decreased linearly from $\omega = 0.9$ to 0.4 [18]. The full second-order RSM was the single-objective fitness function. The search domain was restricted to the tested controller-setting space (I: 5-11; V: 50-70 V; T_{on}: 3-7), with elastic boundary reflection. Convergence was declared when the best-fitness improvement was below 10^{-6} for 10 consecutive iterations.

After optimization, three independent confirmation trials were performed at the model-selected setting. Each trial machined a separate cylindrical cavity of 12 mm nominal diameter and 2 mm depth under the same fixed controller and flushing settings. MRR was calculated using Equation (1), and the three values were summarized by their arithmetic mean and sample standard deviation.

3. Results and Discussions

3.1. Experimental Results Overview

The MRR values recorded across the 27 unique L_{27} conditions are presented in Table 2. The observed range spans 0.97 mm³/min (run 1: I = 5, V = 50 V, T_{on} = 3) to 37.70 mm³/min (runs 19-21: I = 11 and T_{on} = 3), representing an approximately 39-fold variation across the tested space. At I = 5, MRR remains below 2.5 mm³/min regardless of V or T_{on}. Increasing the current-rate index from 5 to 8 and then to 11 produces a strongly accelerating increase in mean MRR, consistent with current-controlled thermal erosion reported for EDM [1, 23, 24].

Table 2. L_{27} design matrix (I and time on are controller indices) and measured MRR values

No.	I (index)	V (V)	T_{on} (index)	MRR (mm³/min)
1	5	50	3	0.97
2	5	60	3	1.03
3	5	70	3	1.1
4	5	50	5	1.97
5	5	60	5	2.43
6	5	70	5	1.87
7	5	50	7	1.32
8	5	60	7	1.35
9	5	70	7	1.43
10	8	50	3	11.9
11	8	60	3	11.9
12	8	70	3	10.77
13	8	50	5	10.28
14	8	60	5	9.42
15	8	70	5	8.7
16	8	50	7	9.05
17	8	60	7	8.38
18	8	70	7	8.08
19	11	50	3	37.7
20	11	60	3	37.7
21	11	70	3	37.7
22	11	50	5	37.24
23	11	60	5	32.31
24	11	70	5	32.31
25	11	50	7	32.31
26	11	60	7	35.4
27	11	70	7	32.31

3.2. Response Surface Model Adequacy

The fitted full second-order RSM achieved $R^2 = 0.995$ and Adj-$R^2 = 0.993$. Leave-one-out PRESS analysis gave Pred-$R^2 = 0.988$, close to Adj-R^2 and therefore supportive of predictive stability within the tested domain. Because no design point was replicated, no pure-error lack-of-fit inference is reported. The agreement between measured and fitted values in Fig. 1 and the influence diagnostics provide complementary checks of model behavior.

Residuals were centered around zero, and Cook's distance remained below 1 for all runs. These diagnostics did not identify an influential observation that would dominate the fitted response. Accordingly, the model is used as an in-domain predictive surrogate; no claim is made for extrapolation beyond the controller-setting ranges investigated.

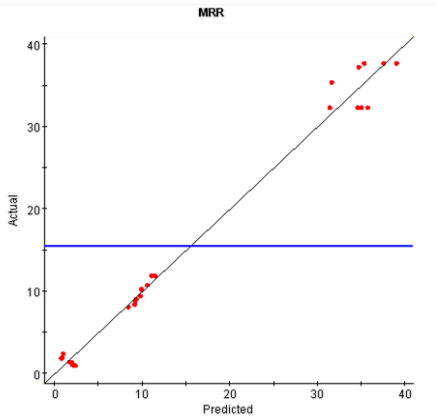


Fig. 1. Predicted versus experimental MRR: goodness-of-fit evaluation of the RSM model

In press

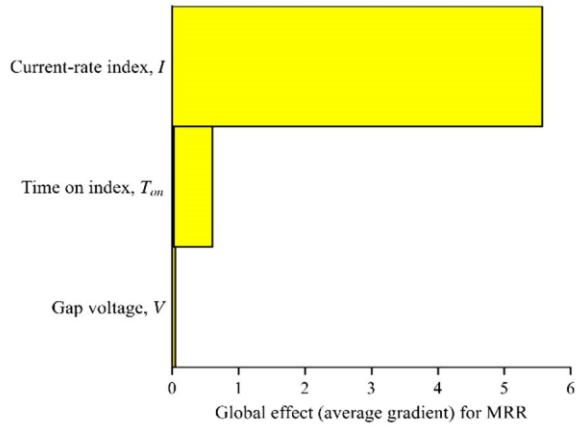


Fig. 2. Main-effect comparison of current-rate index, gap voltage, and time on index for MRR

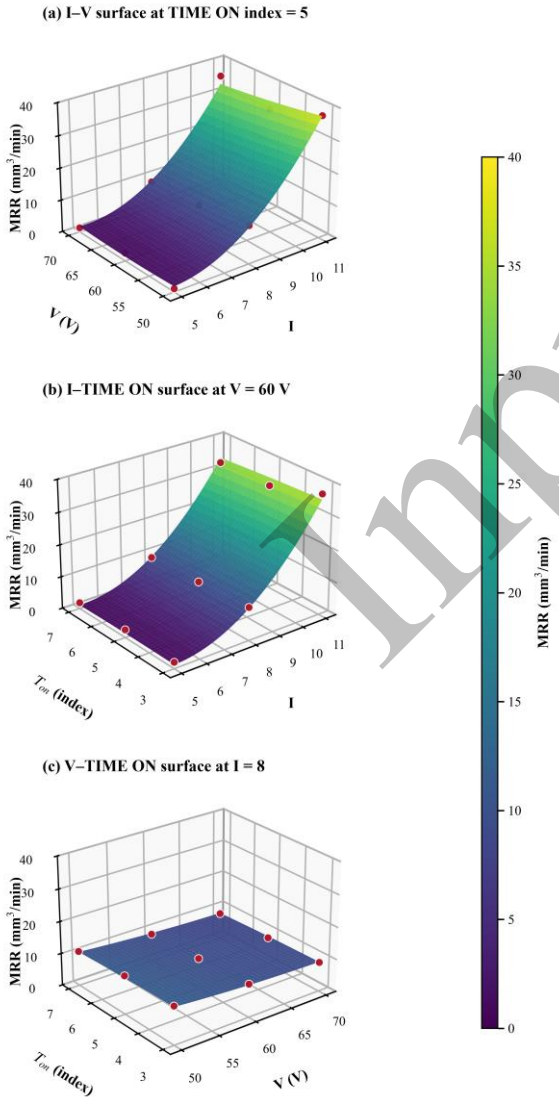


Fig. 3. Full quadratic RSM response surfaces: (a) *I–V* at T_{on} = 5; (b) *I–T*$_{on}$ at *V* = 60 V; and (c) *V–T*$_{on}$ at *I* = 8. Red markers denote submitted experimental points at the stated fixed level

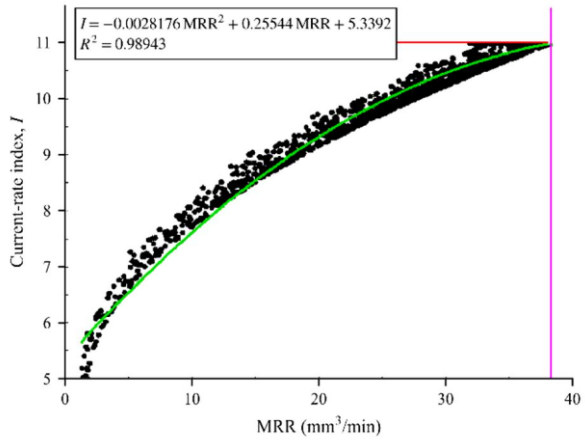


Fig. 4. Quadratic univariate relation between MRR and current-rate index (R^2 = 0.989)

3.3. Main Effects and Physical Interpretation

Regression coefficient analysis identifies current-rate index as the dominant factor governing MRR. In coded units, the current-rate linear coefficient (16.751) is substantially larger in magnitude than those of gap voltage (−0.471) and time on (−1.174). The positive current-rate quadratic coefficient (8.416) captures the accelerating rise in MRR across index levels 5, 8, and 11. This statistical trend is consistent with literature showing that higher discharge-current settings increase the energy delivered per discharge and enlarge the molten region [5, 23, 24].

The positive quadratic term for current-rate index represents convex, rather than plateauing, behavior over the tested levels. Mean MRR increased from 1.50 mm³/min at *I* = 5 to 9.83 mm³/min at *I* = 8 and 35.00 mm³/min at *I* = 11. Plasma-channel expansion, melt formation, and material expulsion reported in prior EDM studies provide a plausible thermo-physical context for this nonlinear trend [5, 6], but these mechanisms are treated here as literature-supported interpretation rather than directly observed phenomena.

Within the investigated range, gap voltage and time on index exerted secondary effects relative to current-rate index. Their coded linear coefficients were both negative (-0.471 for *V* and -1.174 for I_{on}), while the *V* × T_{on} *coefficient was near zero (0.012)*. These model coefficients describe the present machine-setting domain and should not be generalized as universal EDM trends.

3.4. Interaction Effects and Three-Dimensional Response Surface Analysis

The fitted *I* × T_{on} coefficient was negative (-1.173 in coded units), indicating that the MRR gain associated with a higher current-rate index diminished as the time on index increased. Literature models associate prolonged high-energy discharges with plasma-channel

Inpress

expansion, lower peak heat-flux density, partial resolidification, and reduced expulsion efficiency [5, 6]. The observed interaction is consistent with these mechanisms, but the present study did not directly measure plasma dimensions, crater morphology, or resolidified volume.

Debris accumulation and shielding provide a second literature-supported explanation for lower effective removal efficiency at combined high current and time on settings [1]. Because debris concentration and inter-electrode pressure were not measured, this explanation is presented as a plausible interpretation only. The empirical result itself is that the model and the measured data favor the lowest time on index when current-rate index is at its upper tested level.

The three response surfaces in Fig. 3 visualize the complete set of two-factor combinations while holding the third factor at its center level. The *I*-*V* and *I*-T_{on} surfaces show the strong convex rise with current-rate index, whereas the *V*–T_{on} surface at $I = 8$ is comparatively shallow. The negative $I \times V$ and $I \times T_{on}$ coefficients tilt the high-current region toward lower V and lower T_{on}, while the near-zero $V \times T_{on}$ coefficient produces little two-factor curvature in panel (c).

3.5. Particle Swarm Optimization Results

The PSO algorithm converged within 38 iterations to the boundary setting $I = 11$, $V = 50$ V, and $T_{on} = 3$, for which the full RSM predicted MRR = 38.33 mm³/min. Three independent confirmation trials at this setting yielded 37.85, 37.52, and 37.64 mm³/min, giving a mean of 37.67 mm³/min and a sample standard deviation of 0.17 mm³/min. The model overpredicted the confirmation mean by 0.66 mm³/min, or 1.75% relative to the measured mean.

The PSO-selected setting is the same tested corner represented by run 19, rather than an untested interior combination. The confirmation mean is essentially equal to the best L_{27} observation (37.70 mm³/min); therefore, no statistically or practically significant improvement over the experimental optimum is claimed. Here PSO serves to verify the location of the in-domain model maximum and to provide a reproducible search procedure, not to demonstrate a productivity gain beyond the measured design.

Convergence behavior was stable across five PSO runs, each returning the same boundary solution. The optimization remains single-response: it identifies the setting that maximizes MRR within the investigated domain. Surface roughness, electrode wear, and surface integrity were not included in the objective function; their inclusion could shift the practical operating point and should be addressed in a future multi-response study.

4. Conclusion

This study presents a literature-informed RSM–PSO framework for predicting and optimizing MRR in die-sinking EDM of hardened SKD61 steel (50 HRC). The following conclusions are drawn from the experimental and analytical results:

(1) Current-rate index is the dominant factor governing MRR. The positive quadratic coefficient captures the accelerating increase across controller levels 5, 8, and 11; gap voltage and time on index have smaller effects within the ranges investigated.

(2) The negative $I \times T_{on}$ interaction is consistent with literature-described plasma expansion, resolidification, and debris shielding under prolonged high-energy discharge conditions; these mechanisms were not directly measured in this study.

(3) The full quadratic RSM achieved $R^2 = 0.995$, Adj-$R^2 = 0.993$, and Pred-$R^2 = 0.988$. Because the 27 unique conditions were each run once, no pure-error lack-of-fit test was used.

(4) PSO selected $I = 11$, $V = 50$ V, and $T_{on} = 3$, with a predicted MRR of 38.33 mm³/min. Three independent confirmation trials produced 37.67 ± 0.17 mm³/min; the 1.75% overprediction supports in-domain predictive use but does not establish an improvement over the best L_{27} result.

(5) The reported optimum is specific to MRR. Surface roughness, electrode wear, and surface integrity were not optimized, so future work should evaluate a multi-response operating window before broader production deployment.

References

[1] K. H. Ho and S. T. Newman, State of the art electrical discharge machining (EDM), International Journal of Machine Tools and Manufacture, vol. 43, iss. 13, pp. 1287–1300, Oct. 2003. https://doi.org/10.1016/S0890-6955(03)00162-7

[2] M. A. Nafi and M. P. Jahan, Functional surface generation by EDM–a review, Micromachines, vol. 14, iss. 1, 2023, Art. no. 115. https://doi.org/10.3390/mi14010115

[3] S. S. Kumar, T. Varol, A. Canakci, S. T. Kumaran, and M. Uthayakumar, A review on the performance of the materials by surface modification through EDM, International Journal of Lightweight Materials and Manufacture, vol. 4, iss. 1, pp. 127–144, Mar. 2021. https://doi.org/10.1016/j.ijlmm.2020.08.002

[4] M. M. Hasan, T. T. Saleh, A. Sophian, M. A. Rahman, T. Huang, and M. S. Mohamed Ali, Experimental modeling techniques in electrical discharge machining (EDM): A review, The International Journal of Advanced Manufacturing Technology, vol. 127, iss. 5–6, pp. 2125–2150, Jul. 2023. https://doi.org/10.1007/s00170-023-11603-x

In press

[5] D. D. DiBitonto, P. T. Eubank, M. R. Patel, and M. A. Barrufet, Theoretical models of the electrical discharge machining process I: A simple cathode erosion model, Journal of Applied Physics, vol. 66, iss. 9, pp. 4095–4103, Nov. 1989. https://doi.org/10.1063/1.343994

[6] P. T. Eubank, M. R. Patel, M. A. Barrufet, and B. Bozkurt, Theoretical models of the electrical discharge machining process III: The variable mass, cylindrical plasma model, Journal of Applied Physics, vol. 73, iss. 11, pp. 7900–7909, Jun. 1993. https://doi.org/10.1063/1.353942

[7] N.-C. Vu, X.-P. Dang, and S.-C. Huang, Multi-objective optimization of hard milling process of AISI H13 in terms of productivity, quality, and cutting energy under nanofluid minimum quantity lubrication condition, Measurement and Control, vol. 54, iss. 5–6, pp. 820–834, May–Jun. 2021. https://doi.org/10.1177/0020294020919457

[8] M. Ay, U. Çaydaş, and A. Haşçalık, Optimization of micro-EDM drilling of Inconel 718 superalloy, The International Journal of Advanced Manufacturing Technology, vol. 66, iss. 5–8, pp. 1015–1023, May 2013. https://doi.org/10.1007/s00170-012-4385-8

[9] M. S. Sohani, V. N. Gaitonde, B. Siddeswarappa, and A. S. Deshpande, Investigations into the effect of tool shapes with size factor consideration in sink electrical discharge machining (EDM) process, The International Journal of Advanced Manufacturing Technology, vol. 45, iss. 11–12, pp. 1131–1145, Dec. 2009. https://doi.org/10.1007/s00170-009-2044-5

[10] I. Puertas, C. J. Luis, and L. Álvarez, Analysis of the influence of EDM parameters on surface quality, MRR and EW of WC–Co, Journal of Materials Processing Technology, vol. 153–154, pp. 1026–1032, Nov. 2004. https://doi.org/10.1016/j.jmatprotec.2004.04.346

[11] M. Kiyak and O. Çakır, Examination of machining parameters on surface roughness in EDM of tool steel, Journal of Materials Processing Technology, vol. 191, iss. 1–3, pp. 141–144, Aug. 2007. https://doi.org/10.1016/j.jmatprotec.2007.03.008

[12] S. S. Habib, Study of the parameters in electrical discharge machining through response surface methodology approach, Applied Mathematical Modelling, vol. 33, iss. 12, pp. 4397–4407, Dec. 2009. https://doi.org/10.1016/j.apm.2009.03.021

[13] S. Gopalakannan and T. Senthilvelan, EDM of cast Al/SiC metal matrix nanocomposites by applying response surface method, The International Journal of Advanced Manufacturing Technology, vol. 67, iss. 1–4, pp. 485–493, Jul. 2013. https://doi.org/10.1007/s00170-012-4499-z

[14] K.-T. Chiang, Modeling and analysis of the effects of machining parameters on the performance characteristics in the EDM process of Al_2O_3+TiC mixed ceramic, The International Journal of Advanced Manufacturing Technology, vol. 37, iss. 5–6, pp. 523–533, May 2008. https://doi.org/10.1007/s00170-007-1002-3

[15] M. K. Pradhan, Estimating the effect of process parameters on MRR, TWR and radial overcut of EDMed AISI D2 tool steel by RSM and GRA coupled with PCA, The International Journal of Advanced Manufacturing Technology, vol. 68, iss. 1–4, pp. 591–605, Sep. 2013. https://doi.org/10.1007/s00170-013-4780-9

[16] S. K. Saha and S. K. Choudhury, Experimental investigation and empirical modeling of the dry electric discharge machining process, International Journal of Machine Tools and Manufacture, vol. 49, iss. 3–4, pp. 297–308, Mar. 2009. https://doi.org/10.1016/j.ijmachtools.2008.10.012

[17] J. Kennedy and R. Eberhart, Particle swarm optimization, in Proceedings of ICNN'95 - International Conference on Neural Networks, Perth, WA, Australia, vol. 4, pp. 1942–1948, Nov.-Dec. 1995. https://doi.org/10.1109/ICNN.1995.488968

[18] X.-P. Dang, Constrained multi-objective optimization of EDM process parameters using kriging model and particle swarm algorithm, Materials and Manufacturing Processes, vol. 33, iss. 4, pp. 397–404, 2018. https://doi.org/10.1080/10426914.2017.1292037

[19] V. Mohankumar, M. S. S. Kumar, A. Karthik, A. K. Bojer, E. Ali, S. S. M. Ghoneim, and A. B. Abou Sharaf, Optimizing EDM process parameters with the use of GRA-based RSM for machining titanium alloy, Results in Engineering, vol. 26, Jun. 2025, Art. no. 104903. https://doi.org/10.1016/j.rineng.2025.104903

[20] S. Kumar and S. C. Jayswal, Machining performance analysis of wire-EDM for machining of titanium alloy using multi-objective optimization and machine learning approach, Proceedings of the Institution of Mechanical Engineers, Part E: Journal of Process Mechanical Engineering, vol. 240, iss. 3, pp. 2897–2910, Jun. 2026. https://doi.org/10.1177/09544089241288009

[21] S. Ullah, H. U. K. Niazi, and A. Tanveer, Techniques used for process optimization of wire electrical discharge machining: A review, Engineering Proceedings, vol. 56, iss. 1, Oct. 2023, Art. no. 118. https://doi.org/10.3390/ASEC2023-15275

[22] D. Pendokhare, K. Kalita, S. Chakraborty, and R. Čep, A comprehensive review of parametric optimization of electrical discharge machining processes using multi-criteria decision-making techniques, Frontiers in Mechanical Engineering, vol. 10, May 2024, Art. no, 1404116. https://doi.org/10.3389/fmech.2024.1404116

[23] S. H. Lee and X. P. Li, Study of the effect of machining parameters on the machining characteristics in electrical discharge machining of tungsten carbide, Journal of Materials Processing Technology, vol. 115, iss. 3, pp. 344–358, Sep. 2001. https://doi.org/10.1016/S0924-0136(01)00992-X

[24] S. Singh, S. Maheshwari, and P. C. Pandey, Some investigations into the electric discharge machining of hardened tool steel using different electrode materials, Journal of Materials Processing Technology, vol. 149, iss. 1–3, pp. 272–277, Jun. 2004. https://doi.org/10.1016/j.jmatprotec.2003.11.046

[25] Daido Steel Co., Ltd., DHA1 (JIS SKD61): Hot work tool steel, Catalog No. SS0901. [Online]. Available: https://daido.co.jp/products_cms/content/wpcontent/uploads/2024/11/dha1_a.pdf. Accessed on: Nov. 3, 2026.

In press